Supporting Information

# Implanted Battery-Free Direct-Current Micro-Power Supply from in vivo Breath Energy Harvesting

Jun Li,[1†] Lei Kang,[2, 3†] Yin Long,[1, 4] Hao Wei,[2, 5] Yanhao Yu,[1] Yizhan Wang,[1] Carolina A. Ferreira,[2] Guang Yao,[1, 4] Ziyi Zhang,[1] Corey Carlos,[1] Lazarus German,[1] Xiaoli Lan,[5] Weibo Cai,[1,2] * and Xudong Wang[1]*

[1] Department of Materials Science and Engineering, University of Wisconsin-Madison, WI, 53706, USA

[2] Department of Radiology and Medical Physics, University of Wisconsin - Madison, WI, 53705, USA

[3] Department of Nuclear Medicine, Peking University First Hospital, Beijing, 100034, China

[4] State Key Laboratory of Electronic Thin Films and Integrated Devices, School of Optoelectronic Information, University of Electronic Science and Technology of China (UESTC), Chengdu 610054, China

[5] Department of Nuclear Medicine, Union Hospital, Tongji Medical College, Huazhong University of Science and Technology, Wuhan 430022, China.

E-mail: xudong.wang@wisc.edu (X.W.) WCai@uwhealth.org (W.C.)

## S1. Figures and Captions

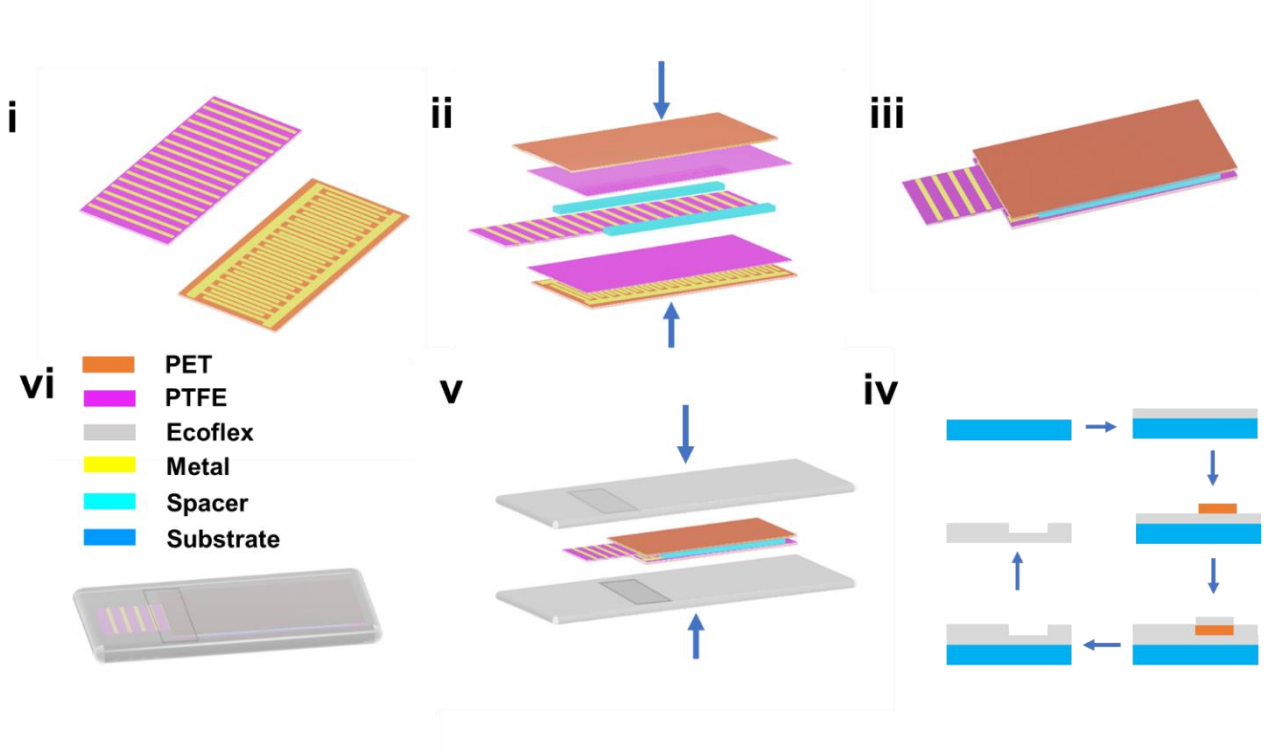


**Figure S1**. ***Preparation of NGs and i-NGs.*** **(i)** Chromium/Copper deposition on PET film and PTFE/PET/PTFE film by metal evaporation. **(ii)** Assembly of NG with multi-layers. **(iii)** As-prepared NG. **(iv)** Fabrication of package layer with cavity pattern by using a PET mask. **(v)** Package of NG by lamination and curing at 60℃ for 1 hour. **(vi)** A final packaged i-NG configuration.

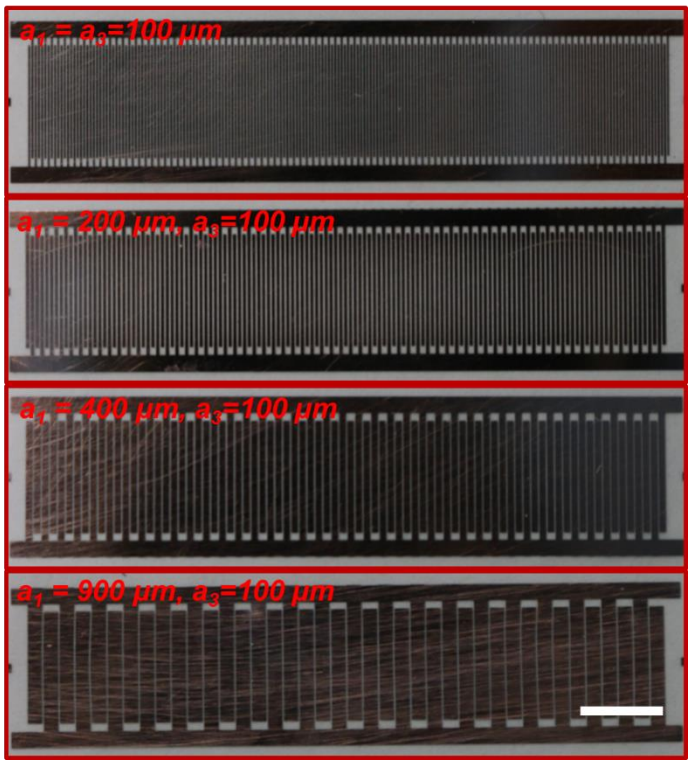


**Figure S2**. Digital photos of interdigital electrodes with four different electrode size configurations. In the images, $a_1$ is the width of electrode finger, $a_3$ is the gap between different eletrode fingers. In all the electrode designs, $a_3$ was remained at a constant 100 μm, while $a_1$ was varied from 100, 200, 400 to 900 (images from top to bottom, respectively). Scale bar is: 1 cm.

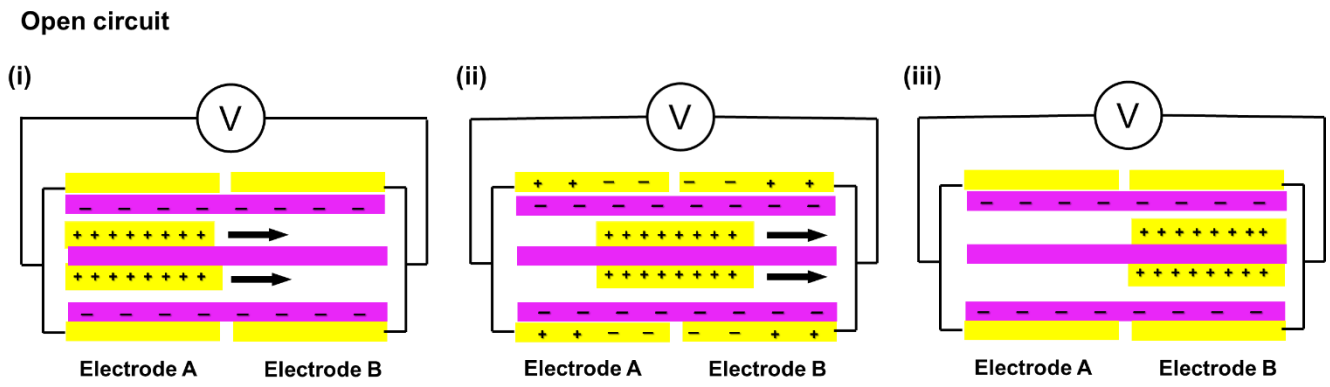


**Figure S3**. ***Voltage generation mechanism.*** Schematic image showing how open-circuit voltage was generated in the sliding i-TENG. **(i)** The initial stage when metal strips were aligned to electrode A which induces the highest potential in electrode A and the lowest potential in the electrode B. **(ii)** The intermediate stage where there is no potential difference between two electrodes. **(iii)** The final stage when metal strips were aligned to electrode B, which induces the highest potential in electrode B but the lowest potential in electrode A.

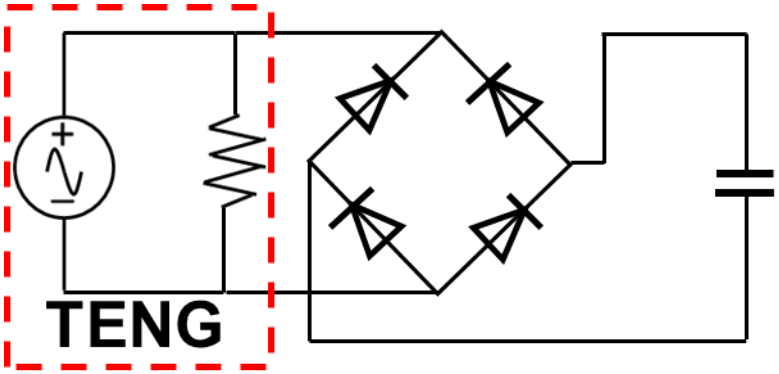


**Figure S4.** Equivalent circuit that was used in the in vitro and in vivo experiments for charging the capacitor by i-TNGE. Circuit in the red box is the equivalent circuit of the i-TENG device.

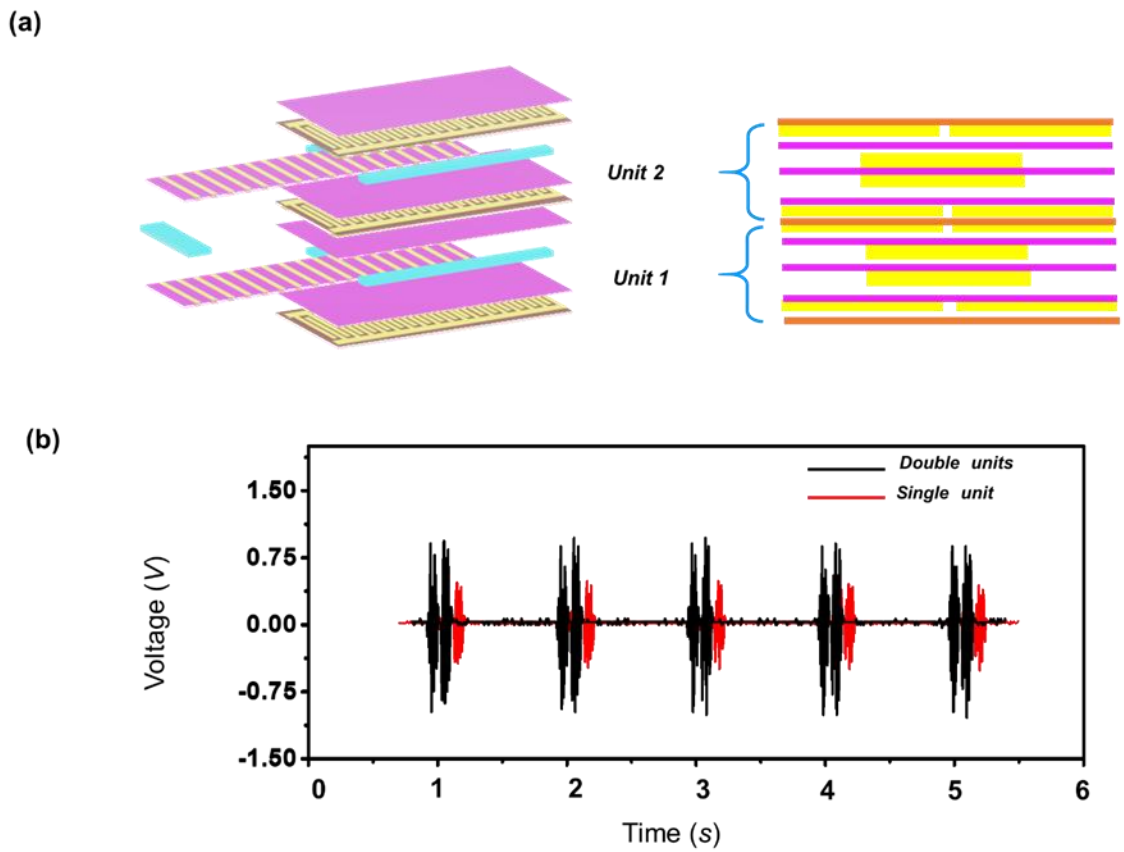


***Figure S5. In vitro electrical characterization***. **(a)** Schematic image of an i-NG assembled by integrating two central triboelectric units to boost the electrical output. The left panel is a 3D illustration of the NG assembly; the right panel is the cross-section of this device. **(b)** The *in vitro* voltage output of i-NGs consists of one (red curves) and two (black curves) triboelectric units driven by a linear motor at a frequency of 1 Hz.

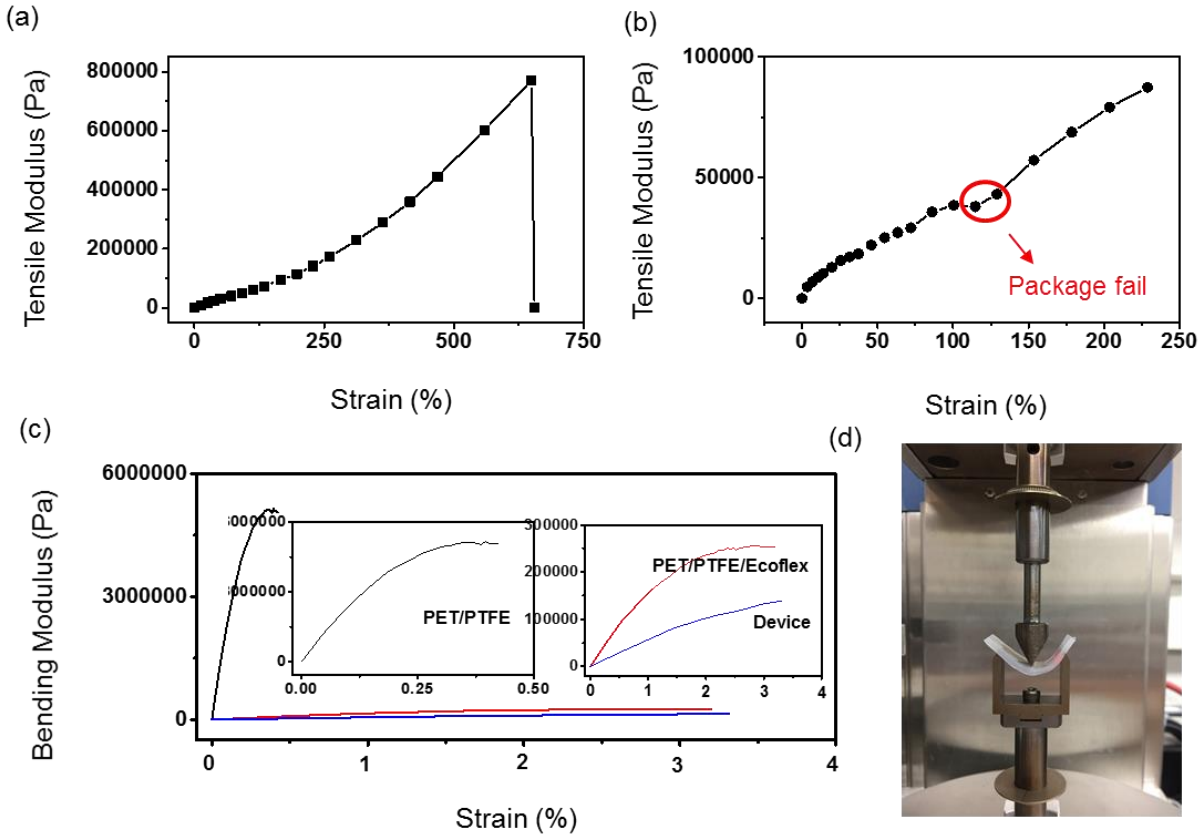


***Figure S6. More mechanical characterizations of as-fabricated i-NG.*** Tensile test of Ecoflex (a) and device (b). (c). Three-point-bending test of PET/PTFE, PET/PTFE packaged by Ecoflex and device. (d). Digital image of bending device under three-point-bending test.

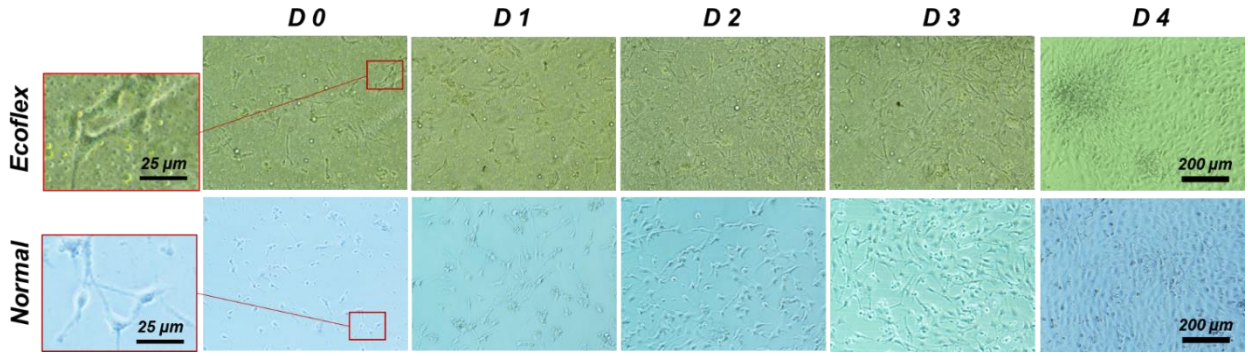


**Figure S7.** ***3T3 fibroblast cells culture***. Optical microscope images of 3T3 fibroblast cells that were cultured on the Ecoflex film (top row) and a standard tissue culture plates (bottom row) for 4 days.

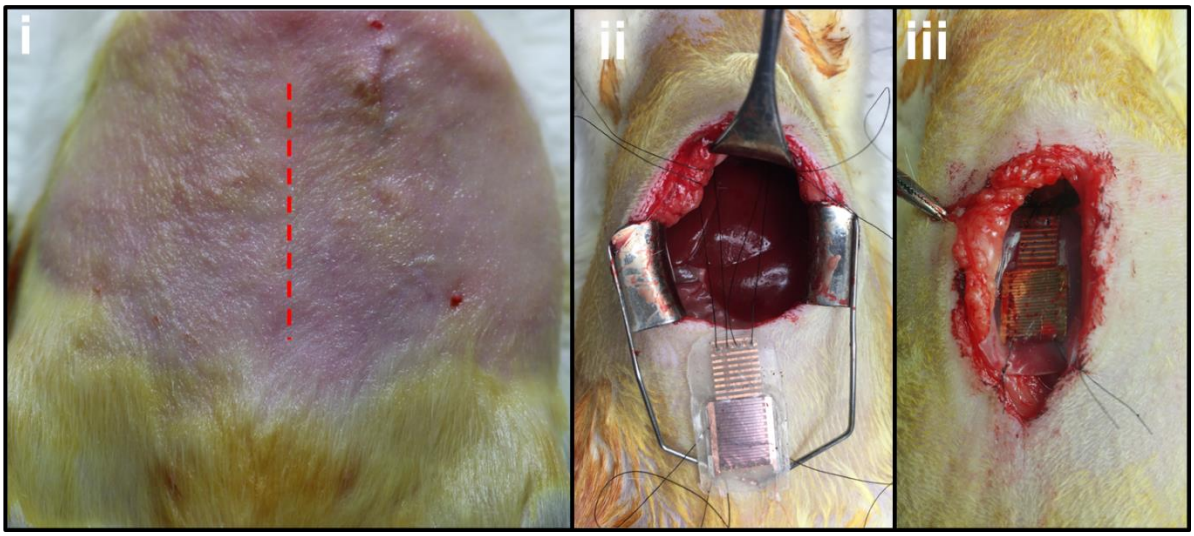


**Figure S8.** ***Surgical process for i-NG implantation***. **(i)** The abdomen of rat was shaved and scrubbed with iodine scrub and alcohol. An incision was made on the area marked with red dashed line. **(ii)** The upper end of i-NG was sutured on both sides of diaphragm central tendon with 2-4 stitches. **(iii)** The bottom end of i-NG was further sutured on the abdominal wall of rat to secure the i-NG.

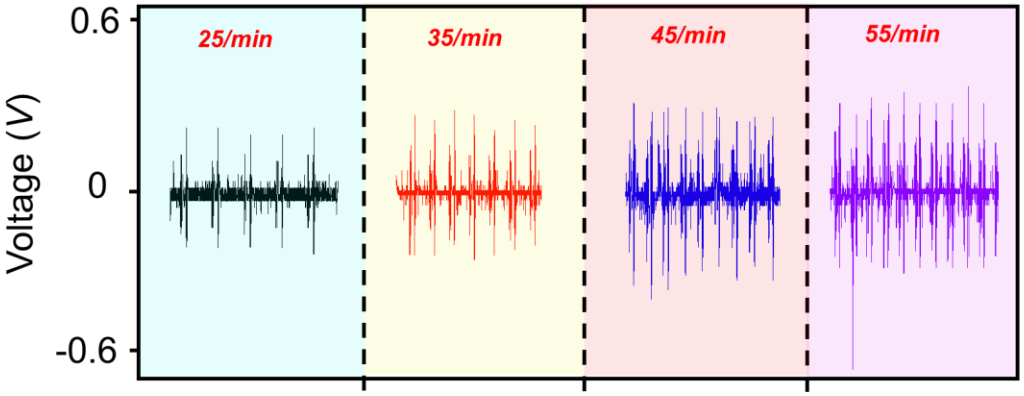


**Figure S9.** ***In vivo output of i-NG***. The voltage outputs of i-NG (consisting of 1 triboelectric unit) driven by the diaphragm motion of rat at difference breathing frequency achieved by controlling the depth of anesthesia.

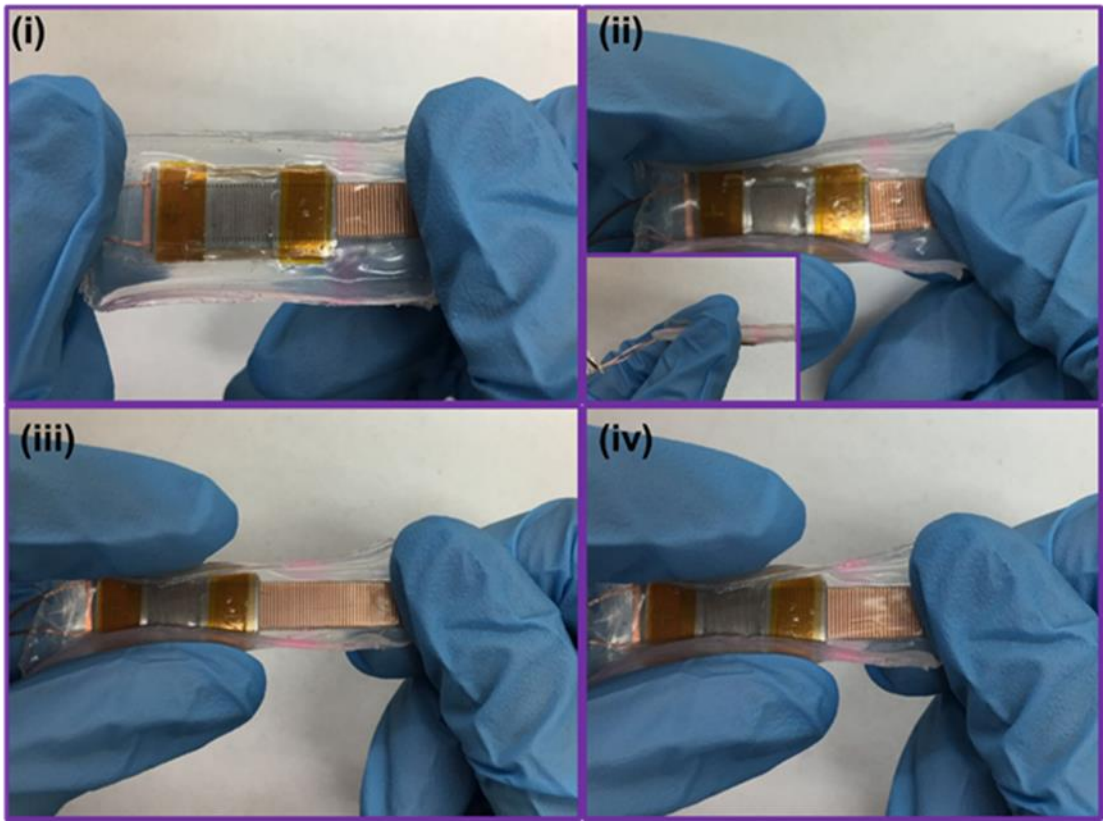


***Figure S10. Warping and i-NG. (i)*** i-NG without warping. ***(ii)*** Warping of iNG. The inset is a side view of warped device. The relatively rigid nature of i-NG will keep it flat while package layer is warped ***(iii)*** I-NG stretched with warping. ***(iv)*** I-NG relaxed with warping

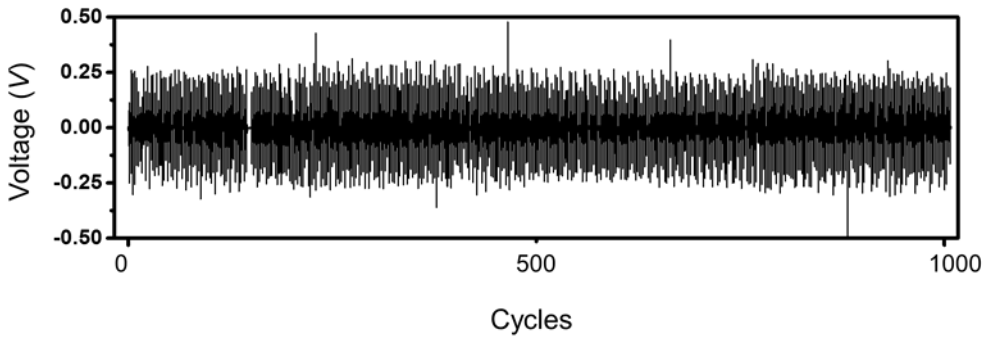


***Figure S11. Stable in vivo output***. A 1000-cycle operation record of i-NG under in vivo, which indicate the good stability of device.

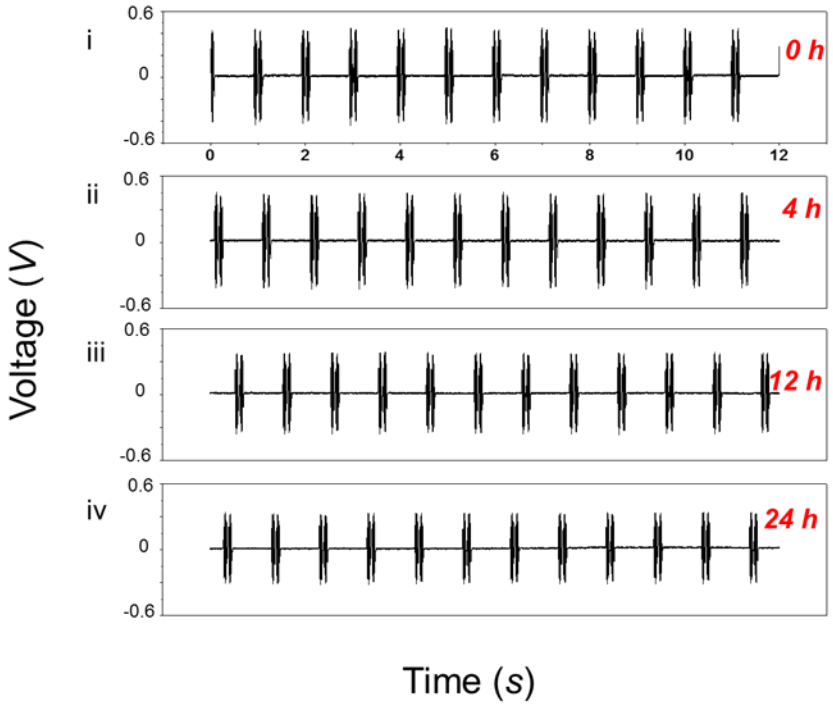


***Figure S12. The evaluation of stability of i-NG in 0.9% NaCl saline solution*** Voltage output of i-NG ***(i)*** before immersed and after immersed ***(ii)*** 4h; ***(iii)*** 12 h; and ***(iv)*** 24 h in saline solution

**Video S1.** Continuously lighting LED by i-NG under stretching motion.

**Video S2**. I-NG activated within rat abdominal cavity by up and down movement of diaphragm.

**Video S3.** In vivo output of single-unit i-NG.

**Video S4.** In vivo direct lighting of LED with blinking.

**Video S5.** Consistent operation of the LED driven by the rat breath

## S2. Tables and Captions

**Table S1.** Power consumption of five typical IMD[1]

| Implants | Power consumption |
|---|---|
| Pacemaker | 5-10 μW |
| Cochlear implant | 100-2000 μW |
| Drug pump | 400 μW |
| Retinal stimulator | 250 mW |
| Neural recording | 1-10 mW |

**Table S2.** Summary of reported i-NG

| NG Configuration | Electrical Output | Animal Model | Implantation site | Ref. |
|---|---|---|---|---|
| ZnO nanowire | $V_{oc}$ of 1-2 mV, $I_{sc}$ of 1-4 pA | Rat | Heart and diaphragm | 2 |
| Contact mode TENG | $V_{oc}$ of 3.74 V, $I_{sc}$ of 0.14 μA | Rat | Chest | 3 |
| $Pb[Zr_xTi_{1-x}]O_3$ ribbons | $V_{oc}$ of ~ 4 V | Bovine, ovine, pig | Heart, lung and diaphragm | 4 |
| PVDF film | V of 0.3 V, $I_{sc}$ of 0.3 μA | Rat | Back region | 5 |
| PVDF film | $V_{oc}$ of 1.5 V, $I_{sc}$ of 300 nA | Pig | Aorta | 6 |
| Contact mode TENG | $V_{oc}$ of 14 V, $I_{sc}$ of 5 μA | Pig | Heart | 7 |
| Contact mode TENG | $V_{oc}$ of 4 - 8 V | Pig | Heart | 8 |
| PMN-PT film | $V_{oc}$ of 17.8 V, $I_{sc}$ of 1.75 μA | Pig | Heart | 9 |
| Biodegradable contact mode TENG | $V_{oc}$ of 4 V | Rat | Subdermal region | 10 |
| This work (micro-grating sliding mode TENG) | V of 0.8 V, $I_{sc}$ of 0.8 μA | Rat | Abdominal cavity | / |

**S3. Calculation of equivalent battery capacity**

Provided that the energy density of fat is 39 kJ/g, while body fat percentage of average person is 25%, the energy stored in fat of an average-weight person (60 kg) is approximately:

$60 \times 25\% \times 10^3 \times 39 \times 10^3 = 5.9 \times 10^8$ J

If a battery has a 3V operating voltage, the capacity is estimated to be:

$5.9 \times 1.0^8 \div 3 \div 3600 = 54629$ A ħ

**S4. Calculation of DC output power**

The DC output from i-NG micro-power supply could be calculated from the charging and discharging curved presented in Fig. 4b. Figure S10 shows the charging and discharging curve in details. Specifically, when i-NG was stretched and relaxed, the generated electricity will charge capacitor (the capacitor discharges through LED at the same time), subsequently, the open-circuit voltage of capacitor rises from 2.12 V at 747.3 s to 2.25 V at 747.5 s. At the interval of i-NG, no electricity from i-NG would be yielded, and the capacitor only discharges through LED. Correspondingly, open-circuit voltage at capacitor drops from 2.25 V at 747.5 s to 2.12 V at 748.3 s. The output power is calculated based on the information as following:

Since the potential drop on capacitor is known, the change of surface charge can be obtained by equation (1):

$$\triangle Q = C \triangle \mathrm{V} \qquad (1)$$

When C is 0.33 μF and potential drop is 0.13 V, the △Q is 0.043 μC. Thus, current flow through LED is estimated by equation (2):

$$I = \frac{\triangle Q}{\triangle t} \qquad (2)$$

△t is 0.8 s in Fig. S6, and then, I is **0.055 μA**. The product of current and average potential gives the estimated output:

$$W = I\,V_{average} \qquad (3)$$

Therefore, W = 0.054 × 2.185 = 0.118 μW

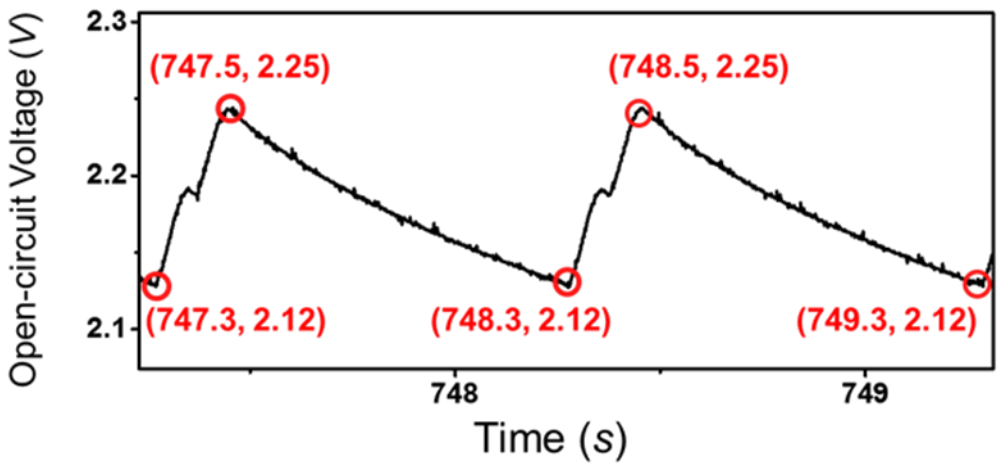


**Figure S13.** Potential profile extrapolated from the fully charged capacitor when connected to the LED load. Potential variation of capacitor.

## References


[1] Yang, Z.; Zhou, S.; Zu, J.; Inman, D., High-Performance Piezoelectric Energy Harvesters and Their Applications. *Joule* 2018.

[2].Li, Z.; Zhu, G.; Yang, R.; Wang, A. C.; Wang, Z. L., Muscle-driven in vivo nanogenerator. *Advanced materials* 2010, 22, 2534-2537.

[3].Zheng, Q.; Shi, B.; Fan, F.; Wang, X.; Yan, L.; Yuan, W.; Wang, S.; Liu, H.; Li, Z.; Wang, Z. L., In vivo powering of pacemaker by breathing-driven implanted triboelectric nanogenerator. *Advanced materials* 2014, 26, 5851-5856.

[4] Dagdeviren, C.; Yang, B. D.; Su, Y.; Tran, P. L.; Joe, P.; Anderson, E.; Xia, J.; Doraiswamy, V.; Dehdashti, B.; Feng, X., Conformal piezoelectric energy harvesting and storage from motions of the heart, lung, and diaphragm. *Proceedings of the National Academy of Sciences* 2014, 111, 1927-1932.

[5] Yu, Y. H.; Sun, H. Y.; Orbay, H.; Chen, F.; England, C. G.; Cai, W. B.; Wang, X. D., Biocompatibility and in vivo operation of implantable mesoporous PVDF-based nanogenerators. *Nano Energy* 2016, 27, 275-281.

[6] Zhang, H.; Zhang, X.-S.; Cheng, X.; Liu, Y.; Han, M.; Xue, X.; Wang, S.; Yang, F.; Smitha, A.; Zhang, H., A flexible and implantable piezoelectric generator harvesting energy from the pulsation of ascending aorta: in vitro and in vivo studies. *Nano Energy* 2015, 12, 296-304.

[7] Zheng, Q.; Zhang, H.; Shi, B.; Xue, X.; Liu, Z.; Jin, Y.; Ma, Y.; Zou, Y.; Wang, X.; An, Z.; Tang, W.; Zhang, W.; Yang, F.; Liu, Y.; Lang, X.; Xu, Z.; Li, Z.; Wang, Z. L., In Vivo Self-Powered Wireless Cardiac Monitoring via Implantable Triboelectric Nanogenerator. *ACS nano* 2016, 10, 6510-8.

[8] Ma, Y.; Zheng, Q.; Liu, Y.; Shi, B.; Xue, X.; Ji, W.; Liu, Z.; Jin, Y.; Zou, Y.; An, Z.; Zhang, W.; Wang, X.; Jiang, W.; Xu, Z.; Wang, Z. L.; Li, Z.; Zhang, H., Self-Powered, One-Stop, and Multifunctional Implantable Triboelectric Active Sensor for Real-Time Biomedical Monitoring. *Nano letters* 2016, 16, 6042-6051.

[9] Kim, D. H.; Shin, H. J.; Lee, H.; Jeong, C. K.; Park, H.; Hwang, G. T.; Lee, H. Y.; Joe, D. J.; Han, J. H.; Lee, S. H., In Vivo Self-Powered Wireless Transmission Using Biocompatible Flexible Energy Harvesters. *Advanced Functional Materials* 2017, 27, 1700341.

[10] Zheng, Q.; Zou, Y.; Zhang, Y.; Liu, Z.; Shi, B.; Wang, X.; Jin, Y.; Ouyang, H.; Li, Z.; Wang, Z. L., Biodegradable triboelectric nanogenerator as a life-time designed implantable power source. *Science advances* 2016, 2, e1501478.